

EXPERIMENTAL AND NUMERICAL INVESTIGATION OF THE BENDING PROPERTIES OF OIL PALM BASED CROSS LAMINATED TIMBER

Martin Hackel¹, Katja Fruehwald-Koenig²

ABSTRACT Increased population figures are leading to higher demand for palm oil and construction products. As a by-product of palm oil production, large quantities of oil palm wood (OPW) are harvested in the near future. The potential of OPW is only utilised to a limited extent. A possible field of application is the use in construction products. The usability of OPW in cross laminated timber (CLT) is therefore being investigated. Lamellas are graded according to their density and dynamic MOE, five-layer (5L) CLT elements are manufactured and subjected to bending tests. In addition, the tests are modelled using the finite element analysis (FEA) and compared with the results of the gamma and shear analogy method. The results of the laboratory tests and analytical methods show good agreement, the results of the FEA overestimate the bending properties (49.3 %) and show their applicability for OPW CLT. A comparison with CLT composed of common wood species shows slightly lower bending parameters for high-performance OPW-CLT. The applicability of OPW in load-bearing building products is confirmed.

KEYWORDS: Cross laminated timber, Oil Palm Wood, elastomechanical properties, Finite Element Analysis (FEA)

1 – INTRODUCTION

Due to population growth and increasing urbanisation worldwide, the demand for multi-storey residential and commercial buildings is increasing significantly. In the same context, the building and construction sector is responsible for around 37% (10 Gt CO₂) of global CO₂ emissions in 2022. The production of building materials such as steel, cement, aluminium, bricks and glass emit 3.7 Gt CO₂ in 2022. In order to achieve the net-zero CO₂ emission targets for new buildings in 2030 and existing buildings in 2050, measures to increase energy efficiency and reduce CO₂ emissions in the production of building materials and buildings are indispensable [1].

The use of renewable resources in the construction sector is one way of helping to achieve the above-mentioned goals. The use of appropriate products, e.g. glulam and cross-laminated timber (CLT) (currently primarily made from traditional wood species), can store CO₂ in the long term. The implementation of various political framework conditions at international level (e.g. the Energy Performance of Buildings Directive (EPBD) of the European Union) continues to lead to increased use of the

products mentioned. To cover the increased demand for building products, alternative raw material sources for the production of these products must be considered.

Due to the above-mentioned global population growth and enhanced consumer behaviour, the demand for raw materials for consumer goods is increasing. As a versatile raw material for the food and chemical industries, palm oil is making an increased contribution to meeting these needs. As a result of these developments, the global area under oil palm cultivation increased by around 9.32 million hectares (48.05 %) to 28.96 million hectares between 2013 and 2023 [2]. A cultivation area of 30 - 40 million ha is forecasted for the year 2030 [3]. At the end of an economic life of 25 - 30 years, oil palm plantations are cleared and replanted [4]. The resulting material is currently only utilised in limited quantities and is primarily used as fertiliser for the next generation of plantations. Annually, up to 180 million m³ (as of 2019) of usable oil palm stem material is produced in the clearing of plantations [3]. The increased areas under cultivation areas are expected to lead to a further increase in material availability. Due to its widespread availability, oil palm stem material offers the potential to

¹ Martin Hackel, Department of Production Engineering and Wood Technology, OWL University of Applied Sciences and Arts, Lemgo, Germany, martin.hackel@th-owl.de

² Katja Fruehwald-Koenig, Department of Production Engineering and Wood Technology, OWL University of Applied Sciences and Arts, Lemgo, Germany, katja.fruehwald@th-owl.de

serve as an alternative raw material for the manufacture of glued load-bearing construction products.

2 – BACKGROUND

Load-bearing construction products like CLT made of oil palm wood are currently not regulated in any standards or similar approvals such as European Technical Assessments (ETA). Glued oil palm products, products made from other monocotyledons or hybrid products made from monocotyledons and common wood species based on board lamellas have only been scientifically investigated to a limited extent. The compression properties perpendicular to the board plane and the indentation properties of three-layer sandwich boards with core layers of oil palm wood (parallel and perpendicular to the board plane) and surface layers of rubberwood are investigated by Srivaro [5]. Srivaro et al. [6] investigate the bending properties of specimens with oil palm core layers and top layers of rubberwood veneer in three-point bending tests with varying spans. Srivaro et al. [7] analyse the compression, rolling shear and hygroscopic properties of pure three-ply oil palm CLT. The thickness of the analysed panels is between 38.5 mm and 44.2 mm. Further investigations of compression and bonding properties, hygroscopic properties and thermal conductivity of three-ply CLT (panel thickness 60 mm) made of coconut palm are carried out by Srivaro et al. [8]. Based on these investigations, Srivaro et al. [9] analyse the compressive and shear strength as well as the bonding properties of other coconut palm and hybrid coconut palm/rubberwood CLT. The specimens are structured in three layers with a target board thickness of 45 mm. Hoffmann [10] investigates the bending and compression properties of five layered hybrid oil palm/bamboo CLT with 84 and 87 mm thickness. Li et al. [11] investigate the bending and shear properties of hybrid bamboo/hem-fir CLT. The shear properties are determined in short span bending tests. The tested specimens are three-layered with varying layups and a panel thickness of 51 mm. Dong et al. [12] also analyse the bending properties of hybrid bamboo/spruce-pine-fir CLT as well as the rolling shear properties. The bending properties are analysed in the form of a static bending test and using the shear analogy method. The analysed panel layups are three- and five-layered with a constant panel thickness of 80 mm. Further investigations on hybrid bamboo/chinese Fir CLT are realised by Zhang et al. [13]. Static bending tests, the shear analogy method, the gamma method and a finite element analysis are used to analyse the bending properties. The shear properties are determined in a short span bending test. The panel

designs are three-layered with varying thicknesses (32 - 58 mm) and layups.

The investigations listed above are limited to comparably small CLT sizes. Furthermore the use of numerical and analytical methods to investigate monocotyledonous based CLT is. Within the scope of this work, the bending properties of five layered OPW-CLT are therefore investigated for the first time experimentally, numerically as well as analytically using a four-point bending test according to DIN EN 16351:2021-06 [14] and DIN EN 408+A1:2012-10 [15], Finite Element Analysis (FEA), shear analogy method and gamma method on test specimens in structural component dimensions.

3 – PROJECT DESCRIPTION

3.1 MATERIAL

3.1.1 Properties of oil palm wood

The stem material of oil palms as monocotyledons differs in its macroscopic structure from common wood species used in construction (dicotyledons). Compared to common wood species, the material of oil palm stems (hereinafter referred to as oil palm wood (OPW)) does not show any wood characteristics such as annual rings (no cambium, no secondary thickness growth), rays, differentiation between heartwood and sapwood or knots. Oil palm wood consists of high-density vascular bundles embedded in a low-density parenchymatous ground tissue [16]. The material can be characterised as a long-fibre reinforced biocomposite. The orientation of the vascular bundles is primarily along the lateral surfaces of the stem, helical orientation can occur [17]. Exceptions are so-called leaf-trace bundles, which serve to supply the palm fronds with nutrients. These are mainly found in the outer area of the trunk and run out of the stem in a curved path [18]. The number of vascular bundles per unit area decreases from the outside to the inside of the stem. A similar progression can be observed over the stem height with increasing numbers of vascular bundles per unit area as the stem height increases [4, 19]. The density of the oil palm wood shows correlations with the number of vascular bundles per unit area and the age of the plant material [4]. The density of the oil palm wood shows a spectrum of 170 kg/m³ in the centre of the stem up to 750 kg/m³ directly below the cortex. The density shows relationships with the distance to the centre of the stem as well as the height of the stem. The elastomechanical properties of oil palm wood show strong, partly power law correlations with the density. Furthermore

elastomechanical properties of oil palm wood are not affected by specimen size due to the mainly influencing factor of its microscopic anatomical structure [20].

3.1.2 Origin

The material on which the present study is based originates from oil palm plantations near Penang, Malaysia. The harvested palms (48 stems) are approximately 30 years old. The stems are cut on a block bandsaw. The boards are kiln dried, but the boiler cannot be heated due to the Covid 19 pandemic lock-down and the original drying schedule cannot be adhered to, which significantly increase the drying defects and has an impact on further processing and recovery rate. A total of 844 boards of varying widths are transported to Germany.

3.1.3 Specimen production

Because of the property variations across the stem cross-section [20, 21], and to reduce the property variations within the individual lamellas, the boards are cut to lamellas with a width of 60 mm using a sliding table saw (Leitz Excellent-Katana saw blade). The lamellas are planed on both face sides using a four-sided planing machine (Weinig-Powermat 600, Leitz HeliPlan planning heads), cross-sectional dimensions of 60 mm x 20 mm are produced. The lamellas are cut to a uniform length of 3000 mm using the sliding table saw. To prepare for subsequent bonding, the lamellas are sanded on both face sides using a wide-belt sanding machine (80 grit sanding). To compensate for slight cross-sectional deformations, the narrow sides are also post-processed using aforementioned four-sided planing machine. The final dimensions of the lamellas are 3,000 x 57 x 19.7 mm.

The density of each lamella is determined in accordance with DIN 52182:1976-09 [22]. The lamellas are graded into one of six density classes (2, 3, 4, 5, 6, 7). Each density class has a range of 100 kg/m^3 (e.g. class 3: $250 \text{ kg/m}^3 \leq \rho < 350 \text{ kg/m}^3$). Due to the availability of raw material, three 5-ply CLT panel layups are produced on an industrial CLT production line from the material of the density classes 4, 5, 6 and 7, with decreasing density from the outer to the inner layers. The numbers corresponding to the density classes, the order of layers is from top to bottom: 6-5-4-5-7 (1 specimen), 6-5-4-5-6 (3 three specimens, and 5-4-4-4-5 (8 specimens). For the evaluation the the specimens are divided into sub-collectives. 6-5-4-5-7 and 6-5-4-5-6 are combined in a higher density sub-collective (designation (+)), 5-4-4-4-5 forms a low density sub-collective (designation (-)). A

one-component PUR adhesive approx. 330 g/m^2 is used for face gluing. Edge gluing is not implemented. The specimens are pressed in a vacuum press at a pressure of 0.8 bar for 180 minutes. The specimens are formatted to the final dimension of 2880 x 600 x 100 mm³. Climatisation at 20 °C and 65 % relative humidity in accordance with DIN 50014:2018-08 [23] cannot be realised due to the dimensions of the test specimens.

3.2 METHODS

The specimens are subjected to a four-point bending test in accordance with DIN EN 16351:2021-06 [14] and DIN EN 408+A1:2012-10 [15]. In addition, these tests are modelled in the form of a finite element analysis (FEA). Furthermore, evaluations are carried out using the shear analogy method and gamma method. The analysed properties include the local modulus of elasticity ($E_{m,l}$), the global modulus of elasticity ($E_{m,g}$), the effective bending stiffness ($(EI)_{eff}$) and the bending strength (f_m). The results are evaluated statistically.

4 – EXPERIMENTAL SETUP

4.1 LABORATORY TEST

The setup of the laboratory tests (Lab) is aligned with the specifications in DIN EN 16351:2021-06 [14] and DIN EN 408+A1:2012-10 [15]. The support distance within the four-point bending test is 2600 mm, so the span/thickness ratio is 26:1 and thus corresponds to the specifications in DIN EN 16351:2021-06 [14] of 24 - 30:1. The distance between the load application points is 650 mm (6.5 h) and thus deviates slightly from the specification of the standards with 6 h (600 mm). The distance from support to load application point with 975 mm (9.75 h) is within the specified range of DIN EN 16351:2021-06 [14] of 9 - 12 h. To determine the local deflection in the non-shear stress area, a support spacing of 500 mm (5 h) is selected in accordance with the above-mentioned standards.

The local and global deflections are recorded using piezoelectric displacement transducers of types 8713-50 (local deflection) and 8713-100 (global deflection) from burster präzisionsmesstechnik GmbH & Co KG. The applied force is recorded by a 150 kN load cell U2 from Hottinger Brüel & Kjaer GmbH with an accuracy of 0.1 %. A QuantumX MX 840A measuring amplifier and the associated MX Assistant V4.12R1 software package from Hottinger Brüel & Kjaer GmbH are used to record the test data. The force increase is controlled manually by operating two control valves.

To calculate the properties to be analysed ($E_{m,l}$, $E_{m,g}$, $(EI)_{CL,local,net}$, f_m), (1) to (4) from DIN EN 408+A1:2012-10 [15] and DIN EN 16351:2021-06 [14] are used.

$$E_{m,l} = \frac{al_l^2 (F_2 - F_1)}{16I(w_2 - w_1)} \quad (1)$$

$$E_{m,g} = \frac{3al^2 - 4a^3}{2bh^3 \left(\frac{w_2 - w_1}{F_2 - F_1} \right)} \quad (2)$$

$$(EI)_{CL,local,net} = E_{m,l}I_{CL,net} = \frac{al_l^2 (F_2 - F_1)}{16(w_2 - w_1)} \quad (3)$$

$$f_m = \frac{3Fa}{bh^2} \quad (4)$$

where $E_{m,l}$ = local MOE, $E_{m,g}$ = global MOE, $(EI)_{CL,local,net}$ = effective bending stiffness, f_m = bending strength, a = distance support, loadpoint, l_l = span support local MOE, $F_2 - F_1$ = load difference in elastic range, I = moment of inertia, $w_2 - w_1$ = deformation difference corresponding to $F_2 - F_1$, l = span global MOE, b = specimen width, h = specimen height, F = maximum load.

4.2 FINITE ELEMENT ANALYSIS

The modelling is realised with the use of the software package ‘Salome Meca 9.10.0 Code_Aster amd AsterStudy portage for Windows’. The basic geometric model of the specimens is implemented as a three-dimensional volume model. To reduce the calculation effort, symmetry properties of the specimens are utilised, making it possible to reduce the size of the volume model to 1/24 of the specimen size. The model consists of five individual layers with the dimensions 1440 x 50 x 20 mm³ (l x w x h) as well as two tabs at support and load points with the dimensions 50 x 50 x 10 mm³ (l x w x h). To further reduce complexity, the individual lamellas are not represented in this study. The layers as single components are meshed individually using hexahedral volume elements with linear approach functions and an element size of 2.5 mm. By applying a compound mesh, a solid bond is created between all components. The adhesive joint is not a part of the presented research.

Orthotropic linear elastic (OPW) and isotropic linear elastic material models (tabs) are used to model the material behaviour. A modulus of elasticity ($E_{steel} = 210,000$ MPa) and a Poisson's ratio ($\mu_{steel} = 0.3$) are defined as material constants for the steel tabs. Nine elastic parameters (E_L , E_R , E_T , G_{LT} , G_{LR} , G_{RT} , μ_{LT} , μ_{LR} , μ_{RT}) are required to describe the orthotropic linear elastic material behaviour. These parameters are assigned to the individual layers according to their average density. To determine the modulus of elasticity in the longitudinal

direction, the relationship established by Fruehwald-Koenig and Heister [24] on compression test specimens in (5) is used for the compression layer. For the remaining layers, the relationship established by Fruehwald-Koenig and Heister [20] in tensile tests is used (6). Due to limited differences in properties along the radial and tangential axis, the same relationship between density and modulus of elasticity is used for both material directions. In the absence of suitable relationships from static tests, the relationship of the modulus of elasticity in the radial direction determined non-destructively by Fruehwald-Koenig et al. [25] in (8) is multiplied by the ratios of the moduli of elasticity in the longitudinal direction in (5) and (6) and the modulus of elasticity in the longitudinal direction determined non-destructively in (7). This serves to compensate for an overestimation of the dynamic elastic properties in dynamic tests. The relationships between density and shear moduli are determined using torsion tests and shown in (9) – (11) [25]. An average value is calculated from the shear moduli of the LR and LT planes, as the exact orientation of the lamellas in the test specimen cannot be reproduced. The Poisson's ratio is not dependent on the density and is defined as $\mu_{LT} = 0.497$, $\mu_{LR} = 0.497$, $\mu_{RT} = 0.117$ [25].

$$E_{c,0} = 0.05773\rho^{1.8922} \quad (5)$$

$$E_{t,0} = 0.0272459\rho^{1.9932} \quad (6)$$

$$E_L = 22.3452\rho + 204.887 \quad (7)$$

$$E_R = 0.318\rho + 223.3798 \quad (8)$$

$$G_{LT} = 1.1175\rho - 275.2169 \quad (9)$$

$$G_{LR} = 1.2489\rho - 280.1694 \quad (10)$$

$$G_{RT} = 0.2727\rho - 19.8083 \quad (11)$$

where $E_{t,0}$ = tensile Young's modulus along the vascular bundles, $E_{c,0}$ = compressive Young's modulus along the vascular bundles, $E_{L,R}$ = Young's moduli along the anatomical axes (ultrasonic test), $G_{LT,LR,RT}$ = shear moduli in symmetry planes, ρ = density.

The boundary conditions of the model are defined by a fixed line support at the support location (degrees of freedom blocked in the x, y and z directions), symmetry conditions on the symmetry plane in the yz plane (translation blocked in the x direction) and the xy plane (translation blocked in the y direction) as well as a forced displacement of the load line at the load location (-10 mm in the z direction). The load is applied in two steps. To determine the global and local deflection, the

displacement components in the z-direction are taken at nodes that correspond to the supports and the measuring points of the laboratory tests. At the load line, the force exerted by the displacement is determined by summing the reaction forces in the z-direction of all nodes in the load line. To calculate the properties to be analysed ($E_{m,l}$, $E_{m,g}$, $(EI)_{eff}$), (1) to (3) from DIN EN 408+A1:2012-10 [15] and DIN EN 16351:2021-06 [14] are used.

4.3 SHEAR ANALOGY

When applying the shear analogy method (SA), (12) is used to calculate the effective bending stiffness [26].

$$(EI)_{eff,y} = \sum_{i=1}^n E_i b_y \frac{t_i^3}{12} + \sum_{i=1}^n E_i b_y t_i z_i^2 \quad (12)$$

where $(EI)_{eff,y}$ = effective bending stiffness, E_i = MOE of i-th layer, b_y = specimen width, n = number of layers, t_i = thickness of laminations in i-th layer, z_i = distance center point i-th layer, neutral axis.

Equations (5) and (6) are used to determine the input parameters for the shear analogy method. Following (3), the local MOE of the specimen can be derived from the effective bending stiffness by division with the moment of inertia of the specimen. The maximum bending strength can be determined by applying (13) (moment bending resistance in CLT slabs) [4] and (14) (maximum bending moment in four-point bending). Equations (13) and (14) are to be equalised and resolved according to the maximum load (15). The bending strength can be determined by inserting the determined maximum load into (4).

$$M_r = F_b \frac{(EI)_{eff}}{E_{mean}} \frac{1}{0.5h} \quad (13)$$

$$M_b = 0.5aF \quad (14)$$

$$F = F_b \frac{(EI)_{eff}}{E_{mean}} \frac{1}{0.5h} \frac{1}{0.5a} \quad (15)$$

where M_r = factored moment bending resistance, F_b = maximum stress (compression lamella), E_{mean} = mean MOE tension layers.

4.4 GAMMA-METHOD

The gamma method (gamma or γ) is used to calculate the effective bending stiffness according to (16) [26].

$$(EI)_{eff,y} = \sum_{i=1}^n E_{yi} I_{yi} + \gamma_i E_{yi} A_i z_i^2 \quad (16)$$

where $(EI)_{eff,y}$ = effective bending stiffness, E_{yi} = MOE of i-th layer, I_{yi} = moment of inertia i-th layer, γ_i = Gamma-factor, A_i = cross section i-th layer, z_i = distance center point i-th layer, neutral axis.

Equations (5) and (6) are used to determine the input parameters for the gamma method. Analogous to the shear analogy method, the local modulus of elasticity can be determined by division with the moment of inertia.

4.5 STATISTICAL ANALYSIS

The mean value, standard deviation (SD), coefficient of variation (COV) and the 5% percentile (5%-P) are determined separately for all specimen collectives (total, (+), (-)) according to test method (Lab, FEA, SA, Gamma) and analysed property ($E_{m,l}$, $E_{m,g}$, $(EI)_{eff}$, f_m). Furthermore, the significance of the differences between the results of the various test methods is analysed. For this purpose, all results are subjected to a normal distribution test. The test is performed separately for each test method (Lab, FEA, SA, Gamma) and specimen collective (total, (+), (-)). The examination for normal distribution is carried out using Shapiro-Wilk and Anderson-Darling tests. In all analyses, no normal distributions can be demonstrated for the total collectives, but normal distributions can be demonstrated for all sub-collectives ((+), (-)). Kruskal-Wallis rank sum tests with pairwise Dunn test with alpha error correction according to Bonferroni or Mann-Whitney-U-test are carried out for the overall collectives to check for significant differences. To test the sub-collectives ((+), (-)), single-factor ANOVAs with subsequent pairwise t-tests with alpha error correction according to Bonferroni or independent t-tests are performed.

5 – RESULTS

5.1 LOCAL MOE

Table 1 shows an overview of the statistical variation parameters of the respective analysis with regard to the local modulus of elasticity. The mean values range from 5,093 MPa (Gamma (-)) to 13,199 MPa (FEA (+)).

The Kruskal-Wallis rank sum test shows significant differences between the investigation methods for the overall collective. The subsequent pairwise Dunn test confirms significant differences between FEA and the other methods. No significant differences are found between laboratory tests, shear analogy and gamma method. The ANOVA and subsequent pairwise t-tests show significant differences between FEA and the other

methods for both sub-collectives. In addition, significant differences between the laboratory tests and the analytical methods are found for the low-density sub-collective.

Figure 1 shows the correlation between the density of the specimens and the local MOE. The analysis is carried out separately according to the panel layup and the test method. The local MOE shows linear correlations with the density in all tests ($R^2 = 0.65 - 0.99$, exception Lab (-) $R^2 = 0.17$). The slopes of the analytical methods differ only slightly, those of the FEA show slightly higher slopes. The slopes of the laboratory tests are considerably higher than those of the comparative methods. In particular, the correlation of the Lab (+) sample is strongly influenced by the results of specimens 1 ($E_{m,l} = 10,155$ MPa) and 4 ($E_{m,l} = 5,626$ MPa), which lead to a high coefficient of variation of 23.91 % within the sample.

Table 1: Statistical variation parameters local MOE

Local MOE				
Method	Mean [MPa]	SD [MPa]	COV [%]	5 %-P [MPa]
Lab	6,722	1,461	21.74	4,318
Lab (+)	7,773	1,859	23.91	4,716
Lab (-)	6,196	963	15.54	4,612
FEA	10,873	1,820	16.74	7,879
FEA (+)	13,199	1,071	8.11	11,438
FEA (-)	9,710	279	2.87	9,252
SA	6,122	1,224	20.00	4,108
SA (+)	7,678	767	9.99	6,417
SA (-)	5,344	169	3.17	5,065
γ	5,818	1,138	19.55	3,946
γ (+)	7,268	692	9.52	6,130
γ (-)	5,093	162	3.18	4,826

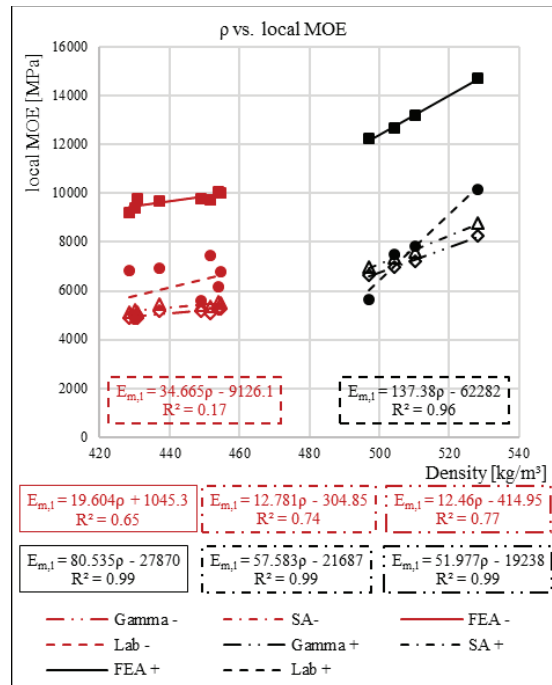


Figure 1: Relationships between density and local MOE

The mean local MOE (Lab) of the total sample $E_{m,l} = 6,722$ MPa is below the local MOE of hybrid bamboo/oil palm CLT $E_{m,l} = 8,000$ MPa determined by Hoffmann [10] and pure hem-fir CLT $E_{m,l} = 10,285$ MPa and in the range of hybrid bamboo/hem-fir CLT reported by Li et al. [11] as well as Radiata Pine CLT $E_{m,l} = 6,350$ MPa reported by Wang et al. [27].

5.2 GLOBAL MOE

Table 2 shows an overview of the statistical variation parameters of the respective analysis with regard to the global modulus of elasticity. The mean values range from 5,401 MPa (Lab (-)) to 14,396 MPa (FEA (+)).

Table 2: Statistical variation parameters global MOE

Global MOE				
Method	Mean [MPa]	SD [MPa]	COV [%]	5 %-P [MPa]
Lab	5,762	1,082	18.79	3,981
Lab (+)	6,483	1,494	23.04	4,026
Lab (-)	5,401	663	12.27	4,311
FEA	12,068	1,824	15.11	9,068
FEA (+)	14,396	994	6.90	12,761
FEA (-)	10,904	399	3.66	10,248

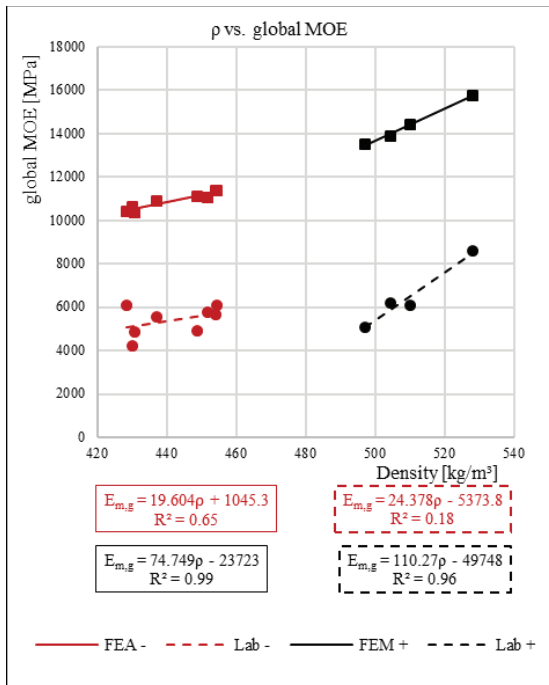


Figure 2: Relationships between density and global MOE

The Mann-Whitney U-test shows significant differences between the test methods for the overall collective. The t-tests show significant differences between FEA and laboratory tests for both sub-collectives.

Fig. 2 shows correlations between the density of the specimens and the global MOE. The global MOE shows linear correlations with the density in all tests ($R^2 = 0.65 - 0.99$, exception Lab (-) $R^2 = 0.18$). The slopes of the FEA relations are slightly below the slopes of the laboratory tests. The correlations differ primarily in the ordinate intercept. The correlation of the Lab (+) test is influenced by the results of specimens 1 ($E_{m,g} = 8,586$ MPa) and 4 ($E_{m,g} = 5,056$ MPa), which lead to a high coefficient of variation of 18.79 % within the sample.

The mean global MOE (Lab) of the total sample $E_{m,g} = 5,762$ MPa is slightly below global MOE of five layered Irish Sitka spruce CLT $E_{m,g} = 6,540$ MPa determined by Sikora et al. [28]. In contrast to the laboratory tests, the FEA for OPW CLT delivers higher results for the global MOE compared to the local MOE. Hackel [29] reports the same effect for OPW glulam.

5.3 EFFECTIVE BENDING STIFFNESS

Table 3 shows an overview of the statistical variation parameters of the respective analysis with regard to the

effective bending stiffness. The mean values range from $2.55E+11$ Nmm² (Gamma (-)) to $6.60E+11$ Nmm² (FEA (+)).

The Kruskal-Wallis rank sum test shows significant differences between the investigation methods for the overall collective. The subsequent pairwise Dunn test confirms significant differences between FEA and the other methods. No significant differences are found between laboratory tests, shear analogy and gamma method. The ANOVA and subsequent pairwise t-tests only show significant differences between FEA and the other methods as well as between the gamma method and the laboratory tests for the low-density sub-collective. No significant differences are found between the investigation methods for the high-density sub-collective.

Table 3: Statistical variation parameters effective bending stiffness

Effective Bending Stiffness				
Method	Mean [10 ¹¹ Nmm ²]	SD [10 ¹¹ Nmm ²]	COV [%]	5 %-P [10 ¹¹ Nmm ²]
Lab	3.84	1.88	48.91	0.751
Lab (+)	4.94	2.93	59.35	.117
Lab (-)	3.30	0.92	27.90	1.78
FEA	5.44	0.91	16.74	3.94
FEA (+)	6.60	0.535	8.11	5.72
FEA (-)	4.86	0.139	2.87	4.63
SA	3.06	0.612	20.00	2.05
SA (+)	3.84	0.383	9.99	3.21
SA (-)	2.67	0.085	3.17	2.53
γ	2.91	0.569	19.55	1.97
γ (+)	3.63	0.346	9.52	3.06
γ (-)	2.55	0.081	3.18	2.41

Fig. 3 shows correlations between the density of the specimens and the effective bending stiffness. The effective bending stiffness shows linear correlations with the density in all investigations ($R^2 = 0.65 - 0.99$, exception Lab (-) $R^2 = 0.18$). The correlations of the analytical methods differ only in their ordinate intercepts; those of the FEA show slightly higher slopes. The slopes of the laboratory tests are considerably higher than those of the comparative methods. In particular, the correlation of the Lab (+) sub-collective is influenced by the result of specimen 1 ($(EI)_{eff} = 9.27E+11$ Nmm²) and 4 ($(EI)_{eff} = 2.81E+11$ Nmm²), which represent the extreme values across all investigation methods and result in a coefficient of variation of 59.35 %.

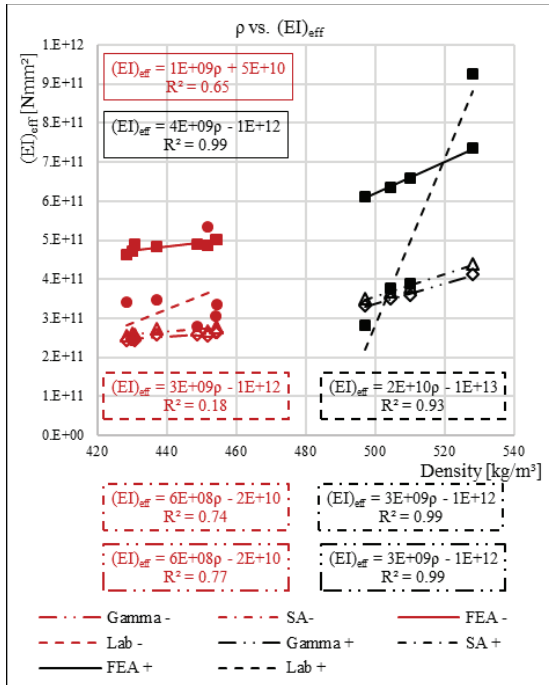


Figure 3: Relationships between density and effective bending stiffness

The effective bending stiffness (Lab) of the total sample $(EI)_{eff} = 3.84E+11$ Nmm² is slightly below the range of the effective bending stiffness $(EI)_{eff} = 5.6E+11$ Nmm² (five layered larch CLT) and $(EI)_{eff} = 4.3E+11$ Nmm² (five layered pine CLT) reported by Pang and Jeong [30]. Furthermore, the results of Pang and Jeong [30] confirm the underestimation of the laboratory results by the shear analogy and gamma method.

5.4 BENDING STRENGTH

Table 4 shows an overview of the statistical variation parameters of the investigations with regard to the bending strength. The mean values range from 19.74 MPa (Gamma (-)) to 30.26 MPa (FEA (+)).

The Kruskal-Wallis rank sum test shows no significant differences between the investigation methods for the overall collective. The ANOVA and subsequent paired t-tests show no significant differences between the investigation methods for the high-density sub-collective. For the low-density sub-collective, significant differences are found between the analytical test methods and the laboratory tests.

Table 4: Statistical variation parameters bending strength

Bending strength				
Method	Mean [MPa]	SD [MPa]	COV [%]	5 %-P [MPa]
Lab	26.99	4.68	17.33	19.30
Lab (+)	28.49	6.42	22.55	17.92
Lab (-)	26.24	3.84	14.64	19.92
SA	23.42	5.36	22.90	14.60
SA (+)	30.26	3.23	10.68	24.95
SA (-)	20.00	0.79	3.93	18.70
γ	23.08	5.23	22.66	14.48
γ (+)	29.77	3.08	10.35	24.70
γ (-)	19.74	0.78	3.97	18.45

Fig. 4 shows correlations between the density of the specimens and the bending strength. The bending strength shows linear correlations with the density in all investigations ($R^2 = 0.79 - 0.99$, exception Lab (-) $R^2 = 0.23$). The correlations of the analytical methods differ primarily in the ordinate intercept; the slopes of the laboratory tests are higher than those of the comparative investigations. In particular, the correlation of the Lab (+) sub-collective is strongly influenced by the results of specimens 1 ($f_m = 37.10$ MPa) and 4 ($f_m = 21.69$ MPa), which represent the extreme values across all investigation methods and lead to a coefficient of variation of 22.55 %.

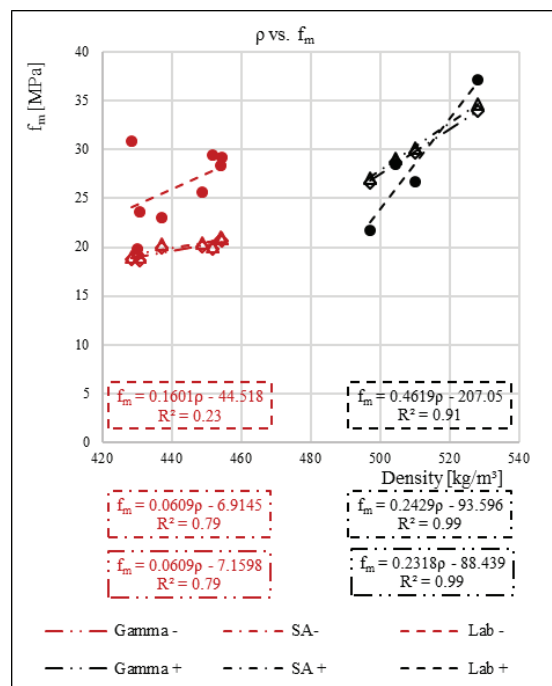


Figure 4: Relationships between density and bending strength

The mean bending strength (Lab) of the total sample $f_m = 28.66$ MPa is in the range of the bending strength of hybrid bamboo/oil palm CLT $f_m = 34.3$ MPa determined by Hoffmann [10] and of hybrid bamboo/hem-fir CLT $f_m = 31.3$ MPa reported by Li et al. [11], but below pure hem-fir CLT $f_m = 47.3$ MPa. The low performance of the test material is due to the relatively low tensile and compressive strengths of the oil palm wood. The results of Hoffmann [10] and Li et al. [11] show that the bending strength can be increased by using materials with higher compressive and tensile strength in the outer layers.

6 – CONCLUSION

Based on the analysis of the results and their comparison with the performance data of CLT from common wood species, the general suitability of using oil palm wood in load-bearing glued construction products (CLT) can be demonstrated. The high variations in the properties, which can be observed, lead to comparatively low statistical variation parameters, which are used as characteristic values for the load-bearing capacity in structural calculations. In order to reduce the variations in the results and possibly achieve better performances, a narrower limitation of the density classes of the raw material should be examined as well as an increased number of specimens. The results of the numerical and analytical investigations confirm the applicability of these methods to determine the behaviour of OPW-CLT to a sufficient extent. Particularly due to the artificial homogenisation in the representation of the specimens, the use of the average density of the individual layers and the corresponding assignment of the material constants, the FEA, shear analogy method and gamma method show considerably low coefficients of variation across all tests and specimen collectives. Particularly in the high-density specimen collective, larger deviations in the numerical and analytical results are recorded, which can be attributed on the one hand to the small sample size and the exceptional behaviour of specimens 1 and 4 on the other. The results of the FEA show significant differences to the laboratory tests. Due to similar slopes of the relationships between density and the investigated properties for FEA, laboratory tests and analytical methods (main differences in ordinate intercept) it is to be pointed out that the results of the FEA can be adjusted by scaling the input parameters. The obtained findings provide starting points for further investigations, in particular the testing of larger specimen collectives and further lay-up variations, as well as the use of additional alternative materials, especially in the surface layers. Furthermore the application of statistically varying

material constants for the representation of larger specimen collectives with an improved representation of lamella property variations within the specimens. The use of alternative material models and plastic material behaviour can be integrated into the FEA so that the flexural strength can be analysed.

7 – REFERENCES

- [1] United Nations Environment Programme, Ed. “2023 Global Status Report for Buildings and Construction.” United Nations Environment Programme, 2024.
- [2] Food and Agriculture Organization of the United Nations. “World wide area harvested of oil palm fruits from 1961 - 2023.”, 2025
- [3] A. Fruehwald and K. Fruehwald-Koenig, “The Use of Oil Palm Trunks for Wood Products,” In: By-Products of Palm Trees and Their Applications (2019), pp. 69–80.
- [4] S. C. Lim and K. C. Khoo, “Characteristics of oil palm trunk and its potential utilization” In: The Malaysian Forester 49.1 (1986).
- [5] S. Srivaro, “Flatwise compressive properties of oil palm core sandwich panel subjected to static compressive load” In: Journal of the Indian Academy of Wood Science 12.2 (2015), pp. 110–115.
- [6] S. Srivaro, N. Matan, and F. Lam, “Stiffness and strength of oil palm wood core sandwich panel under center point bending” In: Materials & Design 84 (2015), pp. 154–162.
- [7] S. Srivaro, N. Matan, and F. Lam, “Performance of cross laminated timber made of oil palm trunk waste for building construction: a pilot study” In: Eur. J. Wood Prod. 77.3 (2019), pp. 353–365.
- [8] S. Srivaro, Z. Pásztor, H. A. Le Duong, H. Lim, S. Jantawee, and J. Tomad, “Physical, mechanical and thermal properties of cross laminated timber made with coconut wood,” Eur. J. Wood Prod. 79.6 (2021), pp. 1519–1529.
- [9] S. Srivaro, H. Lim, M. Li, and Z. Pásztor, “Properties of mixed species/density cross laminated timber made of rubberwood and coconut wood,” In: Structures 40 (2022) pp. 237–246.
- [10] J. Hoffmann, “Investigation on the application of an engineered bamboo board in cross laminated timber,”

Bachelor-Thesis, Rosenheim Technical University of Applied Sciences, Rosenheim, 2018.

[11] H. Li, B. J. Wang, L. Wang, P. Wei, Y. Wei, and P. Wang, "Characterizing engineering performance of bamboo-wood composite cross-laminated timber made from bamboo mat-curtain panel and hem-fir lumber" In: *Composite Structures* 266 (2021), p. 113785.

[12] W. Dong, Z. Wang, J. Zhou, and M. Gong, "Experimental study on bending properties of cross-laminated timber-bamboo composites" In: *Construction and Building Materials* 300 (2021), p. 124313.

[13] X. Zhang, S. Yang, B. Fei, D. Qin, J. Yang, H. Li, X. Wang, "Bending and shear performance of a cross-laminated composite consisting of flattened bamboo board and Chinese fir lumber" In: *Construction and Building Materials*, vol. 392 (2023), p. 131913.

[14] Timber structures – Cross laminated timber – Requirements; German version EN 16351:2021, DIN EN 16351:2021-05, DIN Deutsches Institut für Normung e. V., 2021.

[15] Timber structures – Structural timber and glued laminated timber – Determination of some physical and mechanical properties; German version EN 408:2010+A1:2012, DIN EN 408+A1:2012-10, DIN Deutsches Institut für Normung e. V., 2012.

[16] L. J. Gibson, "The hierarchical structure and mechanics of plant materials," *Journal of the Royal Society*, 2012

[17] P. B. Tomlinson and Horn, J. W., Fisher, J. B., *The anatomy of palms: Arecaceae - Palmae*. Oxford University Press, 2011.

[18] E. S. Bakar, M. H. Sahri, and P. S. H'ng, "Anatomical Characteristics and Utilization of Oil Palm Wood," In: *The formation of wood in tropical forest trees-a challenge from the perspective of functional wood anatomy*, T. Nobuchi and M. H. Sahri, Eds., pp. 161–178 (2008).

[19] L. Fathi, "Structural and mechanical properties of the wood from coconut palms, oil palms and date palms" PhD-Thesis, University of Hamburg, Hamburg, 2014.

[20] K. Fruehwald-Koenig and L. Heister, "Macro- and micromechanical behavior of oil palm wood (*Elaeis guineensis* Jacq.): tensile, compression and bending

properties" In: *Eur. J. Wood Prod.* 82.6 (2024a), pp. 1879–1899.

[21] L. Heister and K. Fruehwald-Koenig, "Glued Laminated Timber from Oil Palm Timber – Beam Structure, Production and Elastomechanical Properties" In: *Proceedings of 2nd World Conference on Byproducts of Palms and Their Applications*, Singapore (2023) pp. 29-44.

[22] Prüfung von Holz - Bestimmung der Rohdichte, DIN 52182:1976-09, DIN Deutsches Institut für Normung e. V., 1976.

[23] Standard atmospheres for conditioning and/or testing — Specifications, DIN 50014:2018-08, DIN Deutsches Institut für Normung e. V., 2018.

[24] K. Fruehwald-Koenig and L. Heister, "Compression properties of glued laminated timber and tensile properties of gluelam lamellas from oil palm wood" In: *Wood Material Science & Engineering* 19.5 (2024b), pp. 1101–1116.

[25] K. Fruehwald-Koenig, B. Faust, and M. Hackel, "Elastic Constants and Shear Strength of Oil Palm Wood (*Elaeis guineensis* JACQ.)" In: *Publication in preparation*, (2025).

[26] E. Karacabeyli and S. Gagnon, *Canadian CLT Handbook: 2019 Edition*, 2019.

[27] Z. Wang, H. Fu, Y. H. Chui, and M. Gong, "Feasibility of using poplar as cross layer to fabricate cross-laminated timber" In: *Proceedings of the World Conference on Timber Engineering*, Quebec 2014, (2014).

[28] K. S. Sikora, D. O. McPolin, and A. M. Harte, "Effects of the thickness of cross-laminated timber (CLT) panels made from Irish Sitka spruce on mechanical performance in bending and shear" In: *Construction and Building Materials* 116 (2016), pp. 141–150.

[29] M. Hackel, "Flexural properties of oil palm wood based glue laminated timber using finite element method" In: *Proceedings of the World Conference on Timber Engineering*, Oslo 2023, (2023).

[30] S.-J. Pang and G. Y. Jeong, "Effects of combinations of lamina grade and thickness, and span-to-depth ratios on bending properties of cross-laminated timber (CLT) floor" In: *Construction and Building Materials* 222 (2019), pp. 142–151.